

Experimental characterization of adobe vaults strengthened with a TRM-based compatible composite

Neda H. Sadeghi¹, Daniel V. Oliveira², Rui A. Silva²,
Nuno Mendes², Mariana Correia³, Hamed Azizi-Bondarabadi⁴

¹ Dept. of Art and Architecture, Yazd University, Yazd, Iran.
e-mail: neda.sadeghi@yazd.ac.ir

² ISISE, Department of Civil Engineering, University of Minho, Guimarães, Portugal.
e-mails: danvco@civil.uminho.pt, ruisilva@civil.uminho.pt, nunomendes@civil.uminho.pt

³ Escola Superior Gallaecia, Vila Nova de Cerveira, Portugal.
e-mail: marianacorreia@esg.pt

⁴ Dept. of Civil Engineering, Yazd University, Yazd, Iran.
e-mail: hamed.azizi@yazd.ac.ir

ABSTRACT:

This paper deals with the structural behaviour and strengthening of adobe vaults representative from historical buildings of the city of Yazd, Iran. Eight destructive tests were performed on 1:3 scaled adobe vault models by loading them at 30% of the span in loading-unloading cycles of increasing vertical displacement. The models were tested considering both unstrengthened and strengthened conditions, where the strengthening consisted of an externally bonded low-cost textile reinforced mortar (LC-TRM) composed of a low-cost fiber-glass mesh embedded in earth-based mortar. Three different strengthening strategies were evaluated, namely by testing undamaged models strengthened at the extrados, undamaged models strengthened at the intrados and repaired models strengthened at the intrados. The experimental results show that the adopted LC-TRM composite improves the structural behavior of adobe vaults, by increasing substantially their load-bearing capacity and by changing the failure mechanism to more ductile ones.

Keywords: Adobe vaults; Experimental characterization; Fiber-glass mesh; Strengthening; Failure mechanisms.

1. Introduction

Adobe vault architecture has more than 3000-year history and refers to a type of construction where adobe walls are erected and roofed by adobe vaults, forming spectacularly complex roofing systems [1]. Arising from the Middle East, this type of architecture has become more mature in this seismically active region of the world. Archaeological excavations confirm that arches and vaults were widely and diversely used in the ancient Middle-East, from southern Egypt to western Persia [2]. Despite the successful use of adobe vault architecture through millennia, its seismic performance is still insufficiently comprehended, since research focused on structural behavior of adobe vaults is scarce in the literature. Vaults built of adobe units and earth-based mortar are generally characterized by a brittle behavior, insufficient connection with adjacent walls and high mass. These factors are detrimental of the structural performance, as they lead vaults to failure even under moderate earthquakes, which has been the cause of several human fatalities in the past [3-8].

The study of the seismic behavior of adobe constructions is mostly related to case studies [4, 9-11], mechanical behavior of adobe units and prisms [12-14], adobe walls [15-17] and scaled adobe structures with wooden pitched or flat roofs [18-22]. On the other hand, most of the studies on the structural behavior of masonry vaults are addressed to stone [23, 24] and brick vaults [25-30].

Iran is located on the Alpine-Himalayan earthquake belt, which is one of the most seismic-prone regions of the world. Still, it holds several vernacular vaulted adobe constructions. Located in the central part of Iran, the city of Yazd is well known due to its integrated adobe residential architecture, recently subscribed as a world heritage site. The peak ground acceleration of Yazd is of about 0.25g for a return period of 475 years [31]. This relatively high seismic hazard combined with the high seismic vulnerability of vaulted adobe constructions are matters of concern regarding the preservation of this heritage and safety of the inhabitants, which justify the need for more detailed research on the seismic behavior of such buildings. It should be noted that prior to seismic research, studying the structural behavior of adobe vaults is essential.

A combined experimental-numerical research project [32, 33] was carried out at University of Minho. The project aimed at evaluating the structural behavior of reference vaults geometrically representative of adobe vaults from the houses of Yazd, considering both the unstrengthened and strengthened conditions. This paper presents and discusses the main results of the experimental program of the project. Within the experimental work, two unstrengthened and six strengthened 1:3 scaled adobe vault models were built and tested. The models were strengthened with a low-cost textile reinforced mortar (LC-TRM) consisting of a low-cost fiber-glass mesh embedded in earth-based mortar.

2. The basics of behavior, strengthening and failure of vaults

2.1 *Behavior and failure mechanisms of masonry vaults*

Comprehensive reviews of historical studies on masonry arches and vaults can be found in Benvenuto [34], Heyman [35], and Carbone, Fiore and Pistone [36], among others. Heyman clearly formalized some hypotheses in order to form the basis for the calculation of arches and vaults from the past centuries [37], by assuming that masonry has zero tensile strength and that

the masonry arch is kept in compression. The concept of the thrust line is used to visualize the forces resultant within arched and vaulted structures. In such a way, an arch or a vault are assumed safe when the thrust line can be drawn totally inside the arch and vault thickness. Cracks develop at the arch and vault due to the movement of trust lines outwards the central core at a given cross-section. Moreover, increasing the load causes to deepen the cracks, which leads to the formation of hinges at the intrados or extrados. The development of a hinge-based mechanism in arched and vaulted structures causes their failure. It should be noted that four hinges are necessary for masonry arches and vaults loaded asymmetrically to form a failure mechanism.

As mentioned, masonry vaulted buildings, especially weak structures such as adobe ones, are vulnerable to earthquakes, see Figure 1a. To study the seismic behavior of arched and vaulted structures, Oppenheim [38] introduced an analytical model describing the masonry arch as a single degree of freedom three-bar (four-hinge) mechanism, see Figure 1b.

In order to analyze the seismic performance of masonry vaults experimentally, a test procedure that contributes to understand their structural performance is the application of a concentrated vertical load at one-third or quarter span. These schemes have a thrusting nature and, due to their action, move the trust line outwards the vault cross-section and develop four hinges that lead to collapse [39], as shown in Figure 1c. It is noteworthy to mention that the typical failure mechanism of masonry vaults submitted to concentrated vertical loads and under the seismic load are approximately similar. In addition, test setups for static load application are much easier, cheaper, faster and more accessible than those for dynamic loading application. Due to these facts, this typology of static tests has been adopted here.

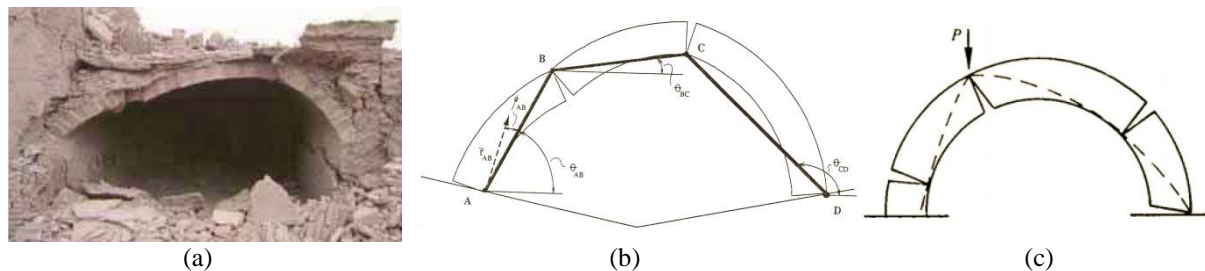


Figure 1. Failure mechanism of vaults: (a) adobe vault after Bam earthquake (2003); (b) masonry vault under seismic load [38]; (c) masonry vault subjected to a concentrated load at quarter-span.

2.2 *Retrofitting techniques for adobe vaults*

Preventing or delaying the collapse of adobe vaults using a suitable strengthening system can be an effective approach for earthquake disaster mitigation regarding these structural elements. Nevertheless, this approach requires development and validation, which can only be achieved through experimental research.

As mentioned before, the literature lacks experimental researches on vaults made of adobe. For instance, adobe arches with different geometries were studied by Oliveira, Varum, Vicente, Sousa and Costa [40]. The arches were tested until collapse under different types of vertical loading, such as distributed symmetrical, distributed non-symmetrical and point load. The results highlighted the influence of the geometry of the arches and loading type on the structural

behavior. The experimental investigation of strengthened adobe vaults has also been addressed by Torrealva, Vargas-Neumann and Blondet [41] by testing two vaulted adobe models on shaking table, one unstrengthened and another strengthened with a polymeric mesh fixed on both sides of the structure. The results revealed that the unstrengthened model was very vulnerable to the applied earthquakes, whereas the strengthened model performed well. Sathiparan and Meguro [42] also assessed the seismic behavior of an adobe house with a vaulted roof strengthened with polypropylene band (PP-band) mesh with or without tie-bars, aiming at evaluating the effects of the two different solutions. To this purpose, shaking table tests were performed on 1:4 scaled models representing both the unstrengthened and strengthened conditions. Both strengthened models evidenced a large improvement of the ductility due to the presence of the PP-band, while the tie-bars only promoted a small improvement on the structural capacity and ductility.

Several traditional strengthening techniques have been applied in the conservation and reconstruction of adobe vaulted constructions, nevertheless the strengthening effectiveness has not yet been studied experimentally for most of the cases. In general, these techniques include: (i) introduction of wooden elements on top of the walls (impost level); (ii) application of steel tie-rods in order to tie parallel walls together to increase the lateral support and to prevent their overturning [43]; (iii) use of steel supporting structures at the intrados [44], (iv) introduction of ring-beams composed of fiber-glass rods introduced on top of the walls and of fiber-glass meshes overlaid by straw earth-based mortar on both sides of the vaults [45]; (v) application of steel-meshes on the extrados covered by gypsum and straw mortar; (vi) use of plastic-mesh strips applied on both sides of the vault and covered with industrial gypsum earth-based mortar; (vii) application of a layer of palm mesh on the extrados; (viii) sewing the vault with palm ropes covered with a straw earth-based mortar plaster [46].

The above-mentioned intervention techniques are expected to improve the structural behavior, and thus the seismic performance of adobe structures in different scales. However, the techniques should respect the following intervention criteria defined for conservation of historic constructions: (i) minimal invasiveness and intervention; (ii) respect authenticity; (iii) respect integrity; (iv) compatibility with original building techniques; (v) reversibility; (vi) durability; (vii) cost-affordable; (viii) based on accessible intervention materials; (ix) feasibility; (x) simple maintenance; (xi) allow monitoring. Among the different strengthening solutions, the application of geogrid meshes and natural fiber meshes embedded in earth-based mortar plasters are intervention techniques that do not only improve the seismic performance of adobe vaults, but also respect most of the criteria listed above.

Despite natural fibers being eco-friendly and compatible with earthen materials, they have some non-negligible limitations, such as swelling-shrinkage behavior due to moisture, lower durability when compared to synthetic meshes, high vulnerability against termite attack, and a poor fire resistance. In fact, the susceptibility of natural fibers to water requires their impregnation or coating, typically performed with epoxy or polyester resins, when used as a reinforcement in earthen plasters, for sake of durability and long-term mechanical performance. Unfortunately, this procedure compromises the eco-friendly value, compatibility and cost of natural fibers reinforcements [47]. Furthermore, natural fibers can be more expensive than synthetic meshes in cities located in arid regions, such as Yazd. Thus, it was decided to adopt an earth-based mortar and a low-cost synthetic mesh as the textile reinforced mortar solution proposed to strengthen the adobe vaults from Yazd.

3. Experimental program

A comprehensive experimental program was conducted to evaluate the structural behavior and seismic strengthening of vaulted adobe houses from Yazd, which was divided into three main phases. The first phase consisted in the definition of a representative composition for the adobes used as units for the vaults, as well as the subsequent production of the scaled adobes. The second phase addressed the experimental work dedicated to the characterization of the mechanical properties of the materials and adobe masonry. Finally, the third phase involved a series of non-destructive and destructive tests on unstrengthened and strengthened adobe vault models. This paper addresses the third phase extensively, while the other two are detailed elsewhere [48].

3.1 Characterization of the materials

The literature concerning the mechanical properties of adobe materials and structures evidences the high dispersion of their values. This issue can be due to differences in the soil used to manufacture the adobes, such as particle size distribution and type of clay, as well as due to differences in the experimental procedure, such as the geometry of the specimens tested, and dissimilar casting and curing conditions. This fact reveals that in order to better analyze the structural performance of adobe structures, it is necessary to experimentally study all components to obtain their mechanical properties.

Within the first phase of the experimental work, a preliminary experimental study was performed in order to produce adobe units for the vault models as representative as possible as those belonging to historical adobe houses from Yazd. It should be noted that transporting the adobes or the raw materials from Iran to Portugal was totally unfeasible, meaning that the adobes could only be produced with local materials. Accordingly, the composition of the adobes was set as 80% of a local sieved soil (≤ 8 mm), 10% of kaolin clay, and 10% of cement (in weight), whereas water was added according to the workability defined by the mason as required to mold the adobes. The bed joint mortar consisted of a mixture of local sieved soil (≤ 2 mm) and kaolin clay with the following weight percentage, respectively: 87% and 13%. The water to solids ratio of the mortar was of about 0.39. This composition was defined after a set of compression tests trials on adobes manufactured with other compositions and dimensions of $270 \times 200 \times 70$ mm³. In the case of the selected composition, the compression tests performed on adobes and masonry prisms (dimensions of $270 \times 200 \times 300$ mm³) allowed to obtain average compressive strength values of 5.32 MPa and 0.90 MPa, respectively (see Figure 2a and Figure 2b). These values are within the ranges reported by Eslami, Ronagh, Mahini and Morshed [14] for adobe masonry from Yazd.

Subsequently to the selection of the composition, 4000 adobes were manufactured in laboratory with reduced scale of 1:3 with dimensions of $90 \times 66 \times 20$ mm³ (see Figure 2c and Figure 2d), which were used to build masonry prisms and reduced scale adobe vault models after curing. Due to the small dimensions of units when compared to the tested adobe units in the pilot experimental work, soil up to 5 mm particle size was applied in the production of the scaled adobe units.

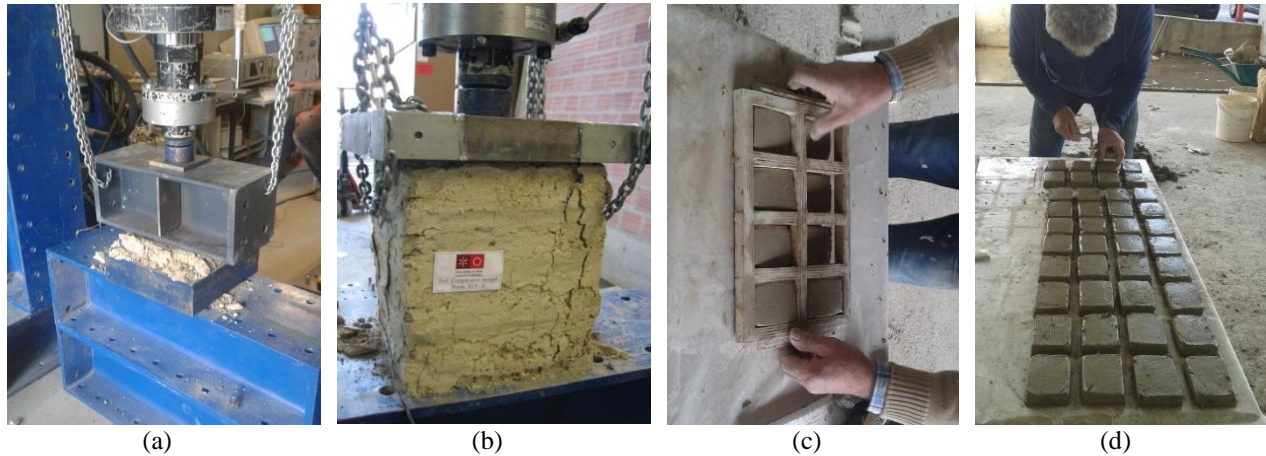


Figure 2. Preliminary experimental study and production of reduced scale adobe units: (a) compression test on adobe; (b) compression test on adobe masonry prism; (c) molding of reduced scale adobes; (d) demolding and drying/curing of reduced scale adobes.

The second phase of the experimental work dealt with the characterization of the mechanical properties of the reduced scale adobes, mortars (bed-joint and strengthening) and masonry. The compressive strength and Young's modulus of the reduced adobes were determined by means of compression tests on cylindrical specimens (100 mm diameter and 200 mm height) casted during the manufacturing. These parameters were also evaluated for the masonry by means of compression tests on prisms (dimensions of $220 \times 100 \times 140 \text{ mm}^3$) representative of the masonry of the vaults. The bed-joint and LC-TRM strengthening mortars were tested under three-point bending and compression according to EN 1015-11 [49]. It should be noted that the strengthening mortar was composed by local sieved soil ($\leq 2 \text{ mm}$), hydraulic lime and kaolin clay in weight percentages of 80%, 10% and 10%, respectively. The water to solids ratio was also of about 0.39, as defined by the experience of the mason.

In addition, the physical and mechanical properties in tension of the LC-TRM reinforcing mesh were characterized. It should be noted that the mesh was selected based on results from a preliminary study, where different local low-cost meshes of different materials (plastic, nylon, steel and glass fibers) were collected and tested to determine their linear density, tensile strength and stiffness [50]. The selection of the mesh took into consideration the cost, performance and application criteria, which led to adopt a fiber-glass mesh with aperture size of $8 \times 9 \text{ mm}^2$ and cost of 0.85 euro/ m^2 . Figure 3 illustrates the execution of the abovementioned tests, while Table 1 summarizes the average values of the obtained mechanical and physical properties.

3.2 Description of the vault models

Most of the adobe houses surveyed in Yazd have vaulted adobe roofs in segmental shape adopting various constructive solutions. The main difference between solutions is related to the space above the vaults, which can include or not infill materials. However, in order to have the flat roofs above the vaults, the space is fully filled with soil or with adobe spandrel walls with small vaults on top (termed as “konou” in Persian architectural literature).

Table 1. Average mechanical and physical properties of the adobe masonry and strengthening materials

Materials	Dimensions [mm]	Compressive strength [MPa]	Tensile strength [kN/m]	Young's modulus [MPa]	Flexural strength [MPa]	Density [kg/m ³]
Adobe masonry (prisms)	220×100×140	0.65	-	480	-	1460
Adobe (cylinders)	∅100×200	1.20	-	792	-	1500
Bed joint mortar (prisms)	160×160×40	0.74	-	-	0.23	1440
Strengthening mortar (prisms)	160×160×40	0.47	-	-	0.19	1360
Fiber-glass mesh	100×400	-	16.8 (x) 12.2 (y)	980 (x) 626 (y)	-	105.3



Figure 3. Characterization of the masonry and strengthening materials: (a) compression test on a cylindrical specimen casted from the adobe mixture; (b) compression tests on strengthening mortar specimen; (c) adobe masonry prism tested under compression; (d) fiber-glass mesh tested under direct tension.

The vaulted adobe roofs are observed in different architectural spaces of an adobe house in Yazd. Among the different spaces, a semi-open, summer-used space, called as “Talar” was selected in this study, since the space exist in most of the houses. Moreover, the vaults used in Talar often present the largest span with respect to the vaults of other spaces. Authors conducted previously a geometric survey of the vaulted roofs used in Talar [33], which allowed to define a reference vault as representative as possible of this typology. The defined reference vault has the span length, rise and thickness of 5700 mm, 1300 mm, and 250 mm, respectively.

Due to technical and economical constrains, it was decided to study the reference vault considering adobe vault models with reduced scale of 1:3, which, for sake of simplicity, resulted in a span, rise and thickness of 1900 mm, 430 mm and 90 mm, respectively (see Figure 4). The width of the adobe vault models was assumed as 450 mm. Aiming at keeping the building process and the test setup as simple as possible, the models were built without infill (soil or

Konou as described before). Hence, the influence of the infill dead load applied at the extrados was not considered in this experimental campaign.

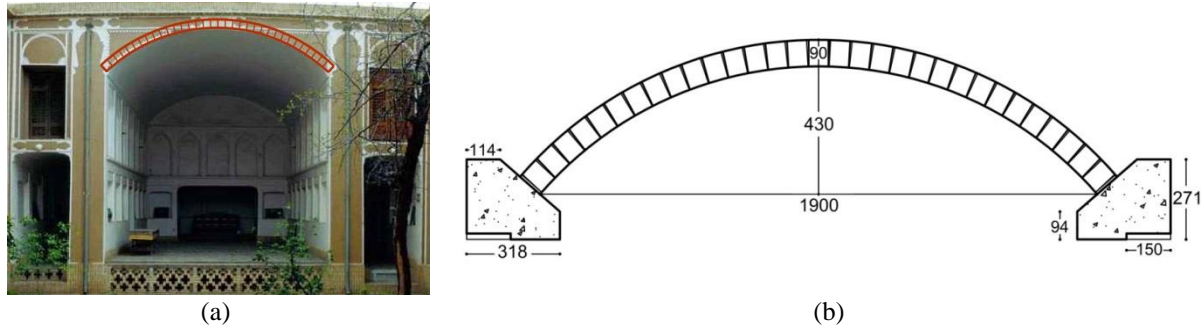


Figure 4. Geometry of adobe vaults: (a) Talar vault from an adobe house of Yazd; (b) reduced scale model.

3.3 Construction and strengthening

Six adobe vaults were built using the reduced scale adobes and bed-joint mortar described previously. The models consisted of 15 circumferential courses with 31-32 adobe units and were built according to the traditional procedure as close as possible. In this procedure, the units are laid perpendicular to the circumferential courses without requiring formwork, as they form inclined arches laid together [5]. However, the absence of local skilled masons, experienced in the procedure of building vaults without formwork, led to adopt a simpler procedure, which included the use of a timber mold. In addition, two concrete blocks casted over rectangular steel plates, were fixed to the laboratory strong floor and used as rigid supports for the models. The construction of each vault model was conducted during two days and the timber mold was carefully removed one week after construction. Figure 5 illustrates the construction of the vault models.

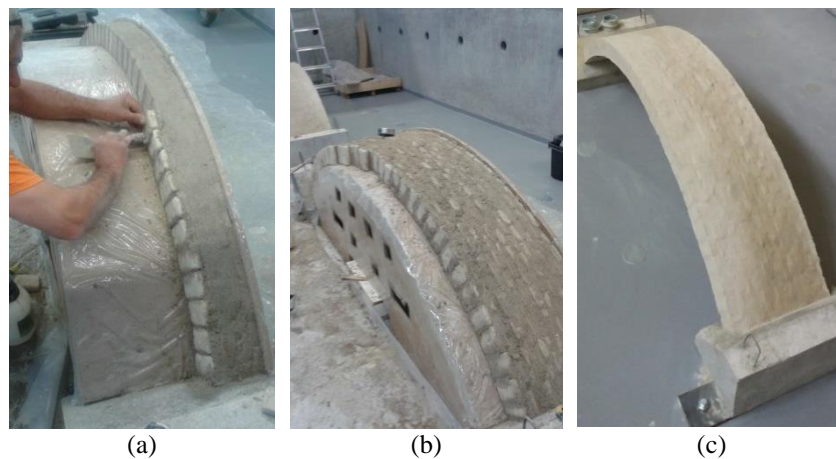


Figure 5. Construction of the adobe vault models: (a) laying an adobe course (b) detail of the formwork; (c) model after removing the formwork.

Four different strengthening conditions of the vaults were tested in the experimental program. The first condition involved the testing of two unstrengthened models (UN1 and UN2), whose results were used as a reference to assess the influence of strengthening on the structural behavior. The other three conditions involved the strengthening of models with a low-cost textile reinforced mortar (LC-TRM), constituted by the fiber-glass mesh and lime earth-based mortar referred previously. The second condition involved the testing of two models strengthened at extrados (SE1 and SE2), while the third involved the testing of two models strengthened at the intrados (SI1 and SI2). The last condition involved the repair and intrados strengthening of the two unstrengthened models after the initial test (DSI1 and DSI2).

The strengthening procedures (strengthening at the extrados and at the intrados) are illustrated in Figure 6. It should be noted that the longitudinal direction of the mesh (x direction) was orientated in the direction of the vaults to grant continuity of the strengthening, thus avoiding mesh overlapping. The application of the strengthening was carried out when the adobe vault models were completely dry. Firstly, the irregularities on the strengthened surface were scrapped with a wire brush to remove loose and protuberant materials, while compressed air was used to remove the generated dust. This procedure aimed at improving the adhesion of the strengthening mortar to the masonry substrate. Then, the strengthened surface was wet by spraying water, in order to prevent excessive water absorption from the strengthening mortar by the vault masonry. Subsequently, the vault was covered with one layer of fiber-glass mesh embedded in two thin layers of strengthening mortar. After flattening the surface of the mortar, the vault was covered with a plastic film for 7 days to mitigate moisture loss by evaporation and promote adequate hydration of the binder. Additional measures were adopted in the models strengthened at the intrados, since detachment of the strengthening layer can more easily occur in this case [28]. Thus, four plate anchors were applied, located at 1/8 and 3/8 of span length on the loaded half-side, and at 1/4 and 3/4 of the vault width (see Figure 6c).

As mentioned before, the unstrengthened vault models (UN1 and UN2) were repaired and strengthened with LC-TRM at the intrados, which allowed to conduct two more tests. These two vaults were firstly moved into their initial undeformed shape and the damaged joints were repaired by repointing with the bed-joint mortar. Afterwards, the vaults were strengthened at the intrados following the same procedure used for the vault models SI1 and SI2. The models were named as DSI1 and DSI2 and were tested up to failure.

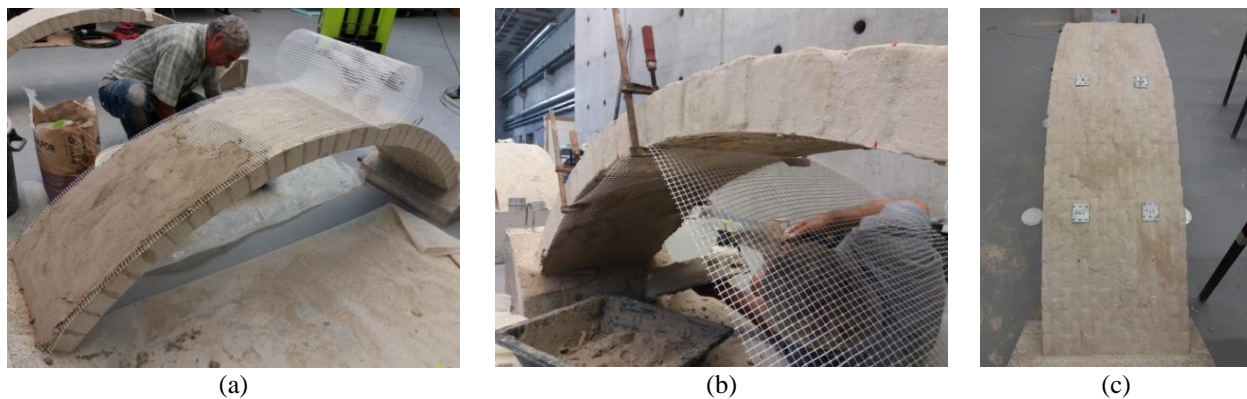


Figure 6. Strengthening of the adobe vault models with LC-TRM: (a) at the extrados; (b) at the intrados; (c) plate anchors applied on a model strengthened at the intrados.

3.4 Test setup and procedure

The loading tests were performed along a series of loading-unloading quasi-static cycles of increasing amplitude of the vertical displacement imposed at about 30% of the vault span, as depicted in Figure 7. The cycle amplitude varied from 0.48 mm to 42 mm, while the displacement rate was of 10-15 $\mu\text{m/s}$ and 10-50 $\mu\text{m/s}$ for loading and unloading, respectively. It should be noted that the rates increased as the amplitude increased in order to keep the duration of the last cycles shorter than 60 min. A quasi-static cyclic procedure was adopted instead of a shaking table test due to the high cost of the latter. This approach allows for an easier identification of the key parameters controlling the structural response of the vault and an adequate calibration of advanced numerical models, which allow predicting the influence of other load configurations and of dynamic effects on the vaults.

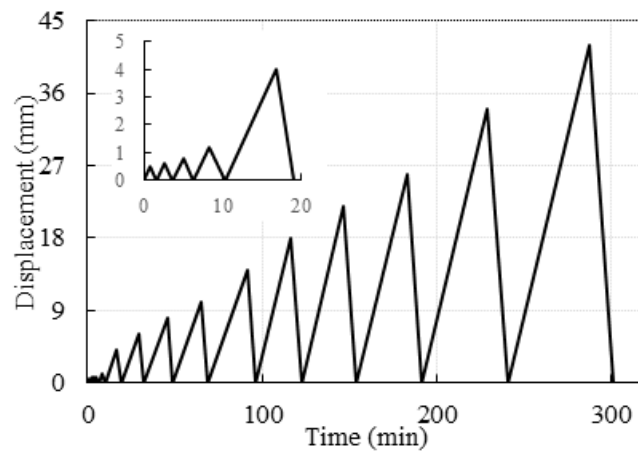


Figure 7. Loading-unloading cycles applied to the vaults.

The load was distributed transversally via a rigid steel beam, which was placed over a timber element shaped according to the curvature of the vault and glued to it. These elements guarantee a uniform loading due to their high stiffness. The load was recorded by means of a 10 kN load cell equipping the loading actuator positioned at mid-width of the vault to reach an uniform transversal loading. In order to improve the initial stress state of the vaults, an additional load of 0.5 kN (consisting of two 25 kg bags) was placed at the mid span.

Eight linear variable differential transducers (LVDTs) were placed at defined locations, aiming at monitoring the vault deflection. Two LVDTs were placed at mid-span and four LVDTs were placed at about 30% of the vault span from both supports. The other two LVDTs were placed at the springers of the vault to control possible displacements at the supports. The layout of the vault test setup is illustrated in Figure 8.

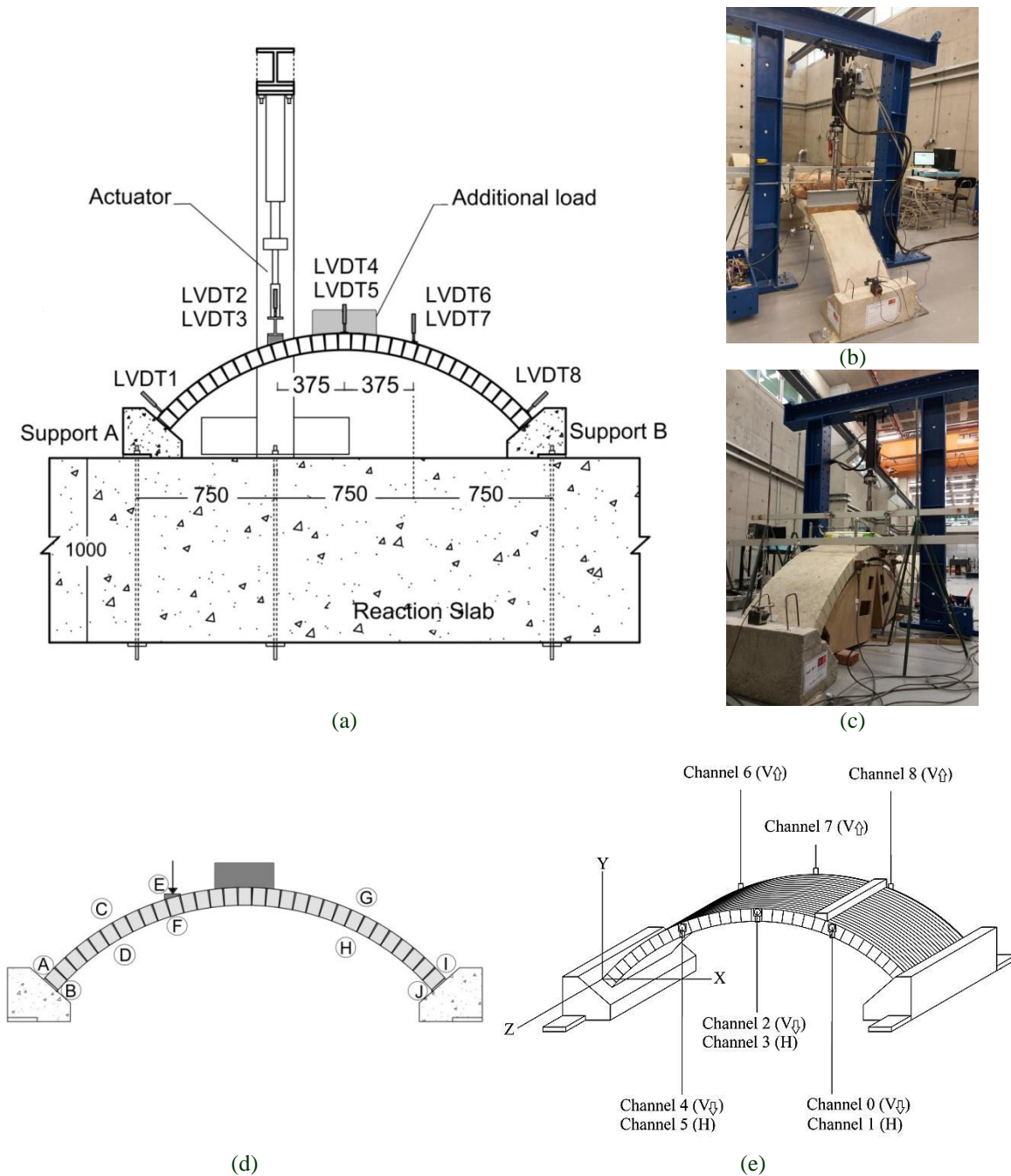


Figure 8. Test setup of the vault models: (a) front view (dimensions in mm); (b) and (c) at laboratory; (d) schematic configuration and location of the critical sections; (e) position and direction of the accelerometers.

Dynamic identification tests were also carried out aiming at estimating the variation of the dynamic properties of the vaults, namely frequencies, as function of the load level applied. It is noted that a reduction in frequency is associated to a reduction of stiffness, which is due to the occurrence of damage (cracking). The ambient vibration was used as source of excitation of the structure and only the response of the structure was recorded (output-only method) [51]. For the dynamic identification tests, nine unidirectional piezoelectric accelerometers (six in the vertical

direction; three in the horizontal direction; bandwidth ranging: 0.15-1000 Hz; dynamic range: ± 0.5 g; sensitivity: 10 V/g), coaxial cables, an acquisition board with 24-bit resolution and acquisition software developed by University of Minho were used (Figure 8e). An identification test before the first loading (initial dynamic properties without damage) and after each loading cycle (dynamic properties after causing possible damage) was done. In total, 84 dynamic identification tests were carried out. The acquisition of the acceleration signals was performed using a sampling frequency of 200 Hz and a total sampling time of 30 min.

4. Test results

In the following sections, the results of the experimental tests carried out on the vault models are grouped according to the strengthening strategy followed. The results are analyzed in terms of stiffness, ductility, deformed shapes, load and deformation capacity, and failure mechanism.

During the tests, a visual inspection of the vaults was continuously performed to register the cracking pattern, as well as the possible detachment of the LC-TRM, hinges location and failure pattern of the vaults. Some initial minor cracks were observed in the vaults before testing due to shrinkage. It should be noted that in the case of models UN1 and UN2, the tests were stopped before failure, which made possible to repair and strengthen them and conduct two more tests (DSI1 and DSI2). Conversely, the strengthened models were tested up to failure. In order to minimize possible damage to test equipment and spreading of debris, few blocks were placed beneath the vaults at an acceptable distance.

4.1 Dynamic properties

The results of the dynamic identification tests were processed in the ARTeMIS software [52] through the Stochastic Subspace Identification (SSI) method [51]. Several frequencies of the vaults were estimated. However, and since the first mode presents higher Modal Assurance Criterion (MAC) values for all dynamic identification tests (higher than 0.95 on average), only the variation of the frequency of the first mode is here evaluated. The first mode of the vaults corresponds to a global bending mode in the vertical direction with the lateral edges out-of-phase (see also Figure 9).

The variation of the frequency of the first mode in the i -th dynamic identification test (f_i) was evaluated with respect to the initial frequency (f_0), estimated during the initial dynamic identification test (DIO). The average of the initial frequency is equal to 23.50 Hz, in which the minimum and maxima values are equal to 21.97 Hz (UN2 and DSI1) and 24.27 Hz (DSI2), respectively (Figure 9). Figure 9 depicts the variation of the frequency ratio (f_i/f_0) averaged for each vault type (UN, SE, SI and DSI) and for all dynamic identification tests. It is noted that the ratios f_i/f_0 present very low variations within each vault type (1.2% on average).

Figure 9 shows that frequency variation ranges from 1.0 to 0.88 for the UN vaults. Since after all the cracks are opened, the stability of the vault is mainly associated to an equilibrium problem without new significant damage, therefore further reduction in the frequencies is not expected (i.e. in the absence of failure, the cracks close after unloading due to the self-weight, not causing variation on the stiffness). The slowest frequency variation occurs for the SE vaults, leading to conclude that the strengthening with LC-TRM at the extrados seems to correspond to

the technique with better mechanical performance. It is noted that these vaults present a very slight increase of the frequency after the first dynamic identification (frequency ratio equal to 1.02), which can be associated with a new internal arrangement of the mortar in the joints due to applied load, causing a slight increase of stiffness. The SI vaults present also a slight improvement in terms of frequency with respect to the unstrengthened vaults (UN). Finally, the frequency variation for the DSI vaults presents a lower reduction in the first dynamic identification tests, but it presents the same reduction as in the last test of the unstrengthened vaults (0.88 in the DI8).

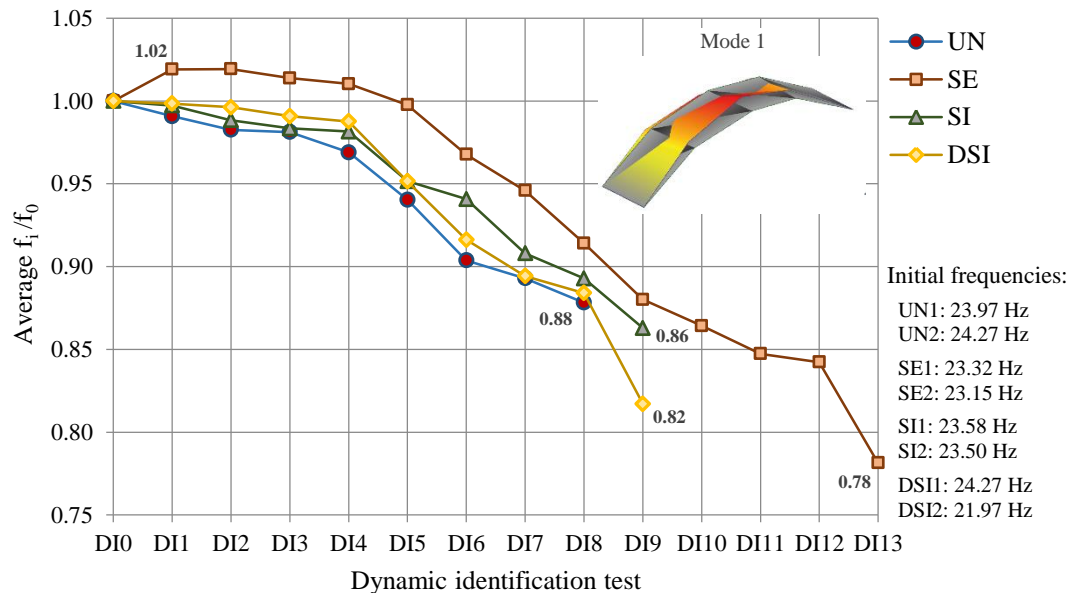


Figure 9. Average frequency variation for the first mode estimated from the dynamic identification tests.

4.2 Unstrengthened vaults

The testing procedure of the two unstrengthened models (UN1 and UN2) included eight loading-unloading cycles. The experimental results show a similar structural behavior between both models, as it can be seen from the cyclic load-displacement curves (and their envelopes) in Figure 10, plotted considering the vertical displacement at the load application section. The maximum load achieved was of 1.13 kN and the maximum displacement was of 15.3 mm for UN1, while those for UN2 were 1.19 kN and 14.6 mm, respectively. The maximum load of both models was achieved in the 5th cycle, being the respective vertical displacement at the load application section of 2.13 mm and 2.70 mm for UN1 and UN2, respectively.

The first visible cracks appeared at the 5th cycle, while an increasing number and depth of cracks were observed in the following cycles. Cracks developed at the sections A, F, G and J (see Figure 8 for the location). The damage development of the unstrengthened models is illustrated in Figure 11. The hinges developed at the load application section (hinge b), at the section in the symmetric side corresponding to 30% span of the vault (hinge c) and at both springers (hinge a and hinge d), as shown in Table 2, where the deformed shape of vaults and the location of the four hinges are portrayed. It should be noted that the discontinuous pattern of the adobe masonry

in the transversal direction of the vaults impeded the formation of the hinges b and c as straight lines.

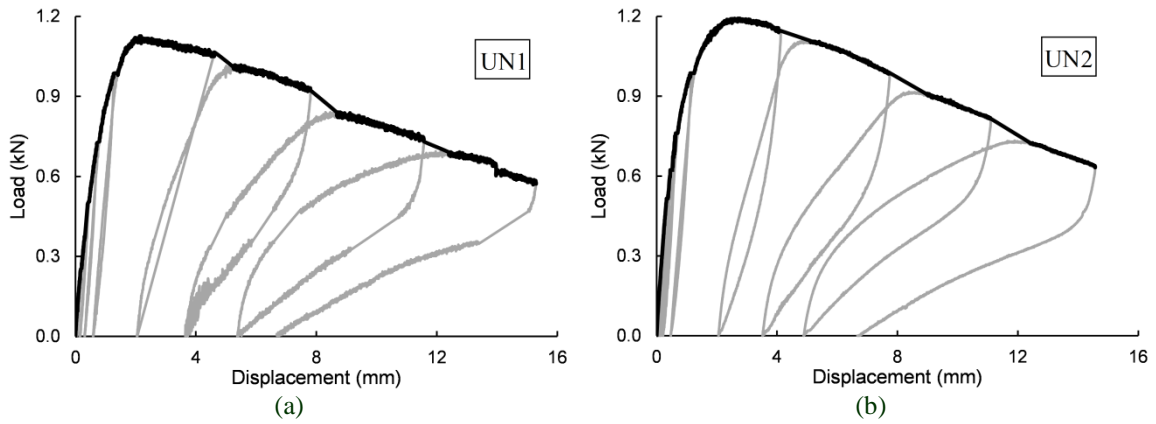


Figure 10. Cyclic load-displacement curves at the loading section and respective envelopes: (a) UN1; (b) UN2.

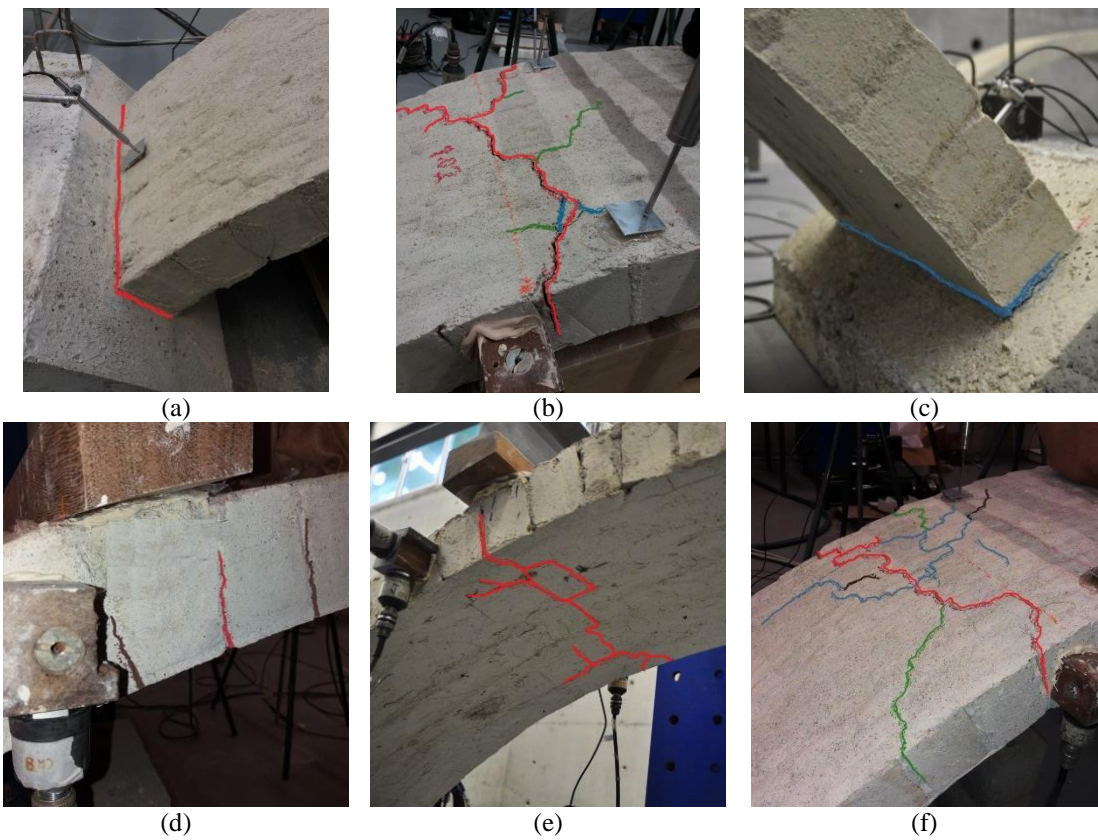


Figure 11. Damage development in the unstrengthened models at the sections: (a) A (UN1); (b) G (UN1) (c) J (UN1); (d) and (e) F (UN2); (f) G (UN2).

4.3 Vaults strengthened at the extrados

The loading tests of the two vault models strengthened at extrados, SE1 and SE2, included twelve and fourteen loading-unloading cycles, respectively. Similarly to the unstrengthened models, the cyclic load-displacement curves (and their envelopes) are presented in Figure 12. The first cracks also appeared in 5th cycle for both vault models, though the maximum load of SE1 was achieved in the 10th cycle and that of SE2 was achieved in the 9th cycle. SE1 attained a maximum load of 2.61 kN and a maximum displacement of 43.4 mm while those achieved by SE2 were 2.72 kN and 63.3 mm, respectively. It should be noted that the maximum load achieved by both models was similar, but SE2 achieved a considerably higher maximum displacement. With respect to the unstrengthened models, the load capacity increased about 125% and 134% for SE1 and SE2, respectively. The displacement at the maximum load also increased substantially, namely 11 and 8 times for SE1 and SE2, respectively. A very important behavior observed in these tests was the long post-peak branch, which allows a significant increase in ductility promoted by the strengthening. An increase of initial stiffness of the vaults was also observed (see Section 5.1 for further details).

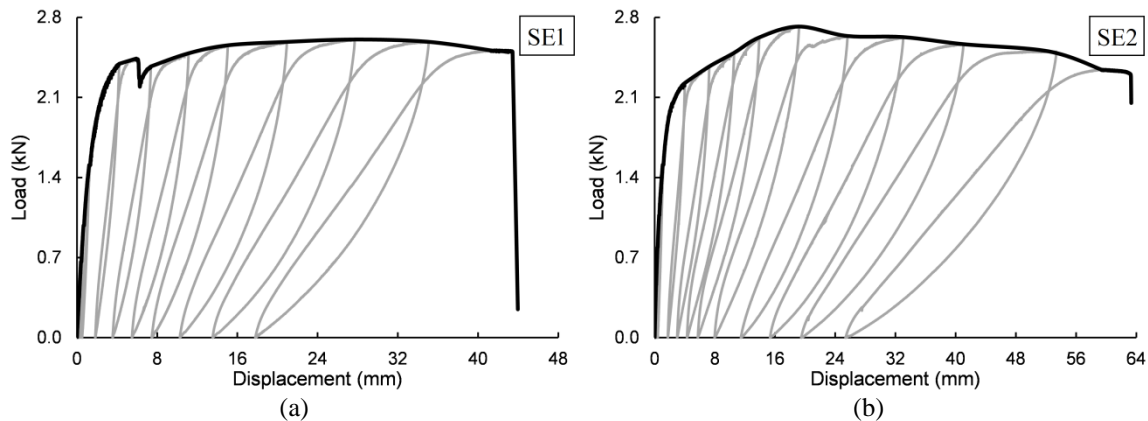


Figure 12. Cyclic load-displacement curves at the loading section and respective envelopes: (a) SE1; (b) SE2.

The development of the failure mechanisms of both models strengthened at the extrados was also very different from the unstrengthened ones. The first cracks appeared beneath the load application section (section F in Figure 8d), which were deepened as the loading test progressed (see Figure 13). The strengthening prevented the opening of a discrete hinge at the extrados. Instead, a distributed crack pattern appeared in the plaster at the symmetric side of the loading and kept spreading towards support B. For instance, Figure 13e illustrates the crack pattern at section G (in Figure 8d) of the model SE2. Cracks also appeared at the springers, namely in the intrados next to support B (Section J in Figure 8d) during the first loading cycles. Cracks also developed at the extrados of the springer next to support A (section A in Figure 8d), though the strengthening clearly postponed the cracking development. Failure occurred due to detachment of strengthening layer, as shown in Figure 13f, which indicates that cohesion between strengthening mortar and adobe masonry was insufficient to develop the full strength of the reinforcing mesh.

In general, both strengthened models present similar structural behavior, nevertheless their failure mechanisms differed slightly. In model SE1, the initial detachment of the strengthening

composite layer occurred at section E (in Figure 8d), while for SE2 the strengthening layer separated from the vault initially near section A (in Figure 8d). Another difference is related to the number of cracks observed at section C (in Figure 8d), in which more cracks were observed for SE1. The strengthening system prevented the four-hinge collapse mechanism to develop. Instead, the vaults developed three hinges and one additional “release” of the LC-TRM strengthening. In other words, the position of the three hinges is similar to that observed for the unstrengthened vaults, namely at the load application section and at both vault springers. The increase in deformation caused the development of cracking from section G to section I (support B in Figure 8a), which eventually led to detachment of the strengthening layer (4th release) and subsequent collapse. The location of hinges and the 4th “release” (R) are depicted in Table 2.

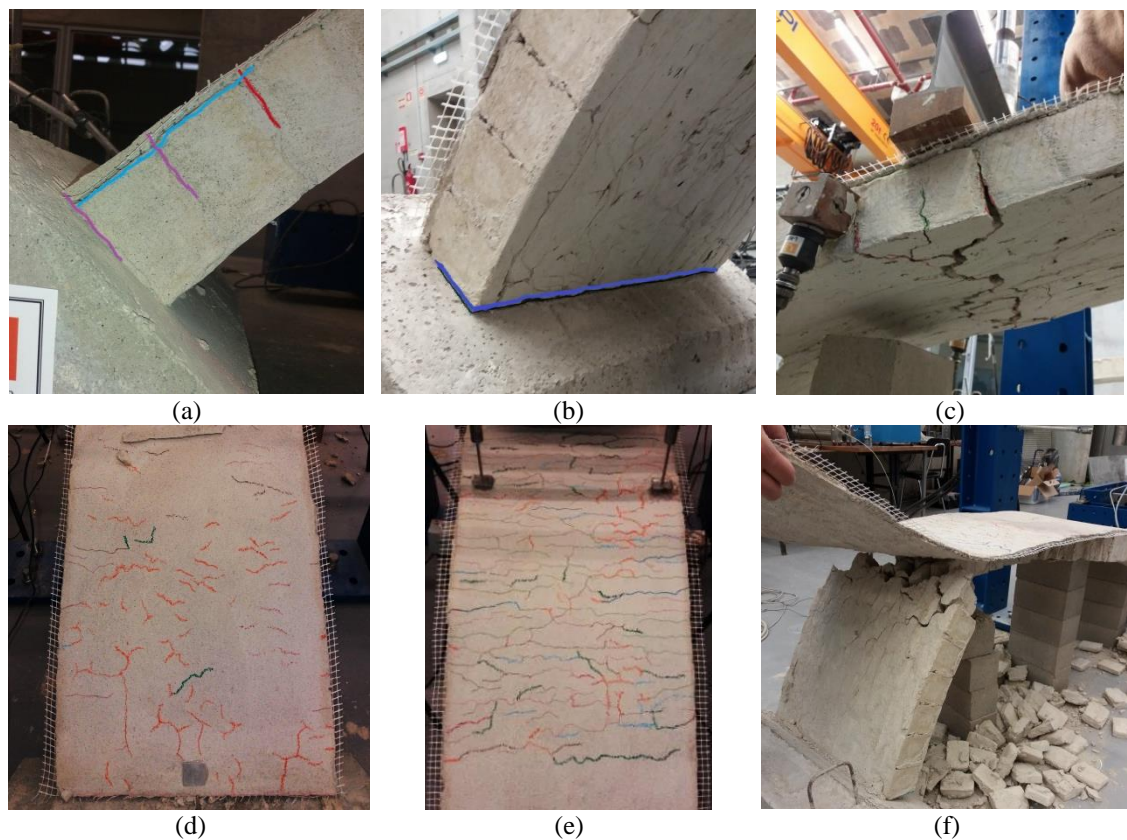


Figure 13. Damage development of the vault models strengthened at the extrados: (a) detachment of strengthening at section A (SE2); (b) cracks at section J (SE1); (c) cracks at section F (SE2); (d) cracks at section C (SE2); (e) cracks at section G (SE2); (f) detachment of strengthening layer at section G and I (SE1).

4.4 *Vaults strengthened at intrados*

The loading tests of the two vault models strengthened at the intrados (SI1 and SI2) included ten loading-unloading cycles. Both the structural behavior and collapse mechanisms of these models differed from those of the models presented in the two previous sections. The cyclic load-displacement curves (and their envelopes) are illustrated in Figure 14, which evidence a similar structural behavior of both vaults. The first cracks occurred during the 5th cycle, while the

maximum load values were obtained in the 6th cycle. SI1 achieved a maximum load equal to 2.66 kN and maximum displacement equal to 23.6 mm, while those achieved by SI2 were 2.39 kN and 22.5 mm, respectively. With respect to the unstrengthened condition, the strengthening at the intrados increased the load capacity of vaults SI1 and SI2 in about 129% and 106%, respectively. The maximum load was also achieved for a displacement 3 and 2.3 times greater for SI1 and SI2, respectively. Furthermore, the ductility increase was significant, though the behavior was more brittle than that of the vault models strengthened at the extrados. It should be noted that the initial stiffness of the models strengthened at intrados also increased with respect to the unstrengthened ones (to be discussed in Section 5.1).

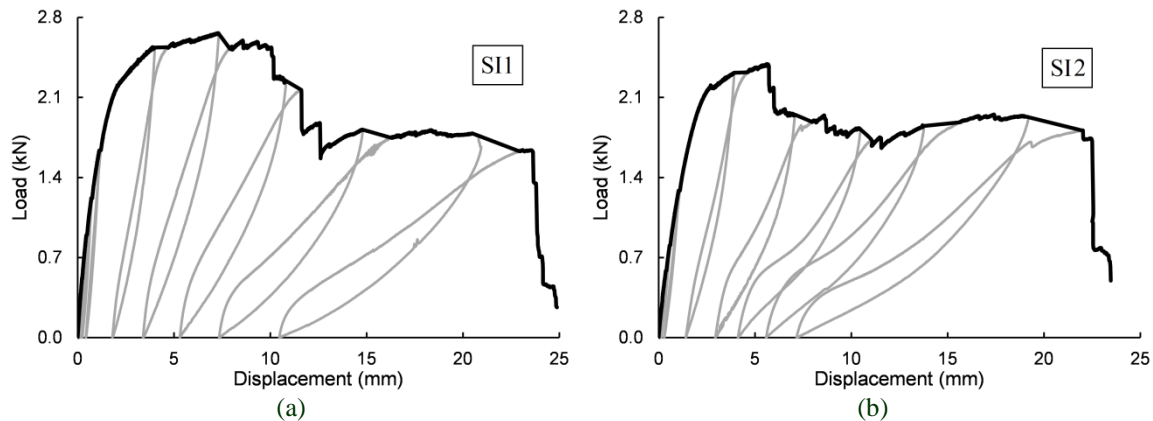


Figure 14. Cyclic load-displacement curves at the loading section and respective envelopes: (a) SI1; (b) SI2.

The failure mechanism development of the SI vaults is illustrated in Figure 15. The first visible cracks appeared at the symmetric side of the load application section (section G in Figure 8d), as shown in Figure 15c. In fact, the strengthening delayed the hinge opening at the intrados of the load application section (section F in Figure 8d) until the onset of the detachment of strengthening layer at this section. In the last loading cycles, the strengthening mortar tended to separate from the fiber-glass mesh. It is worth noting that the sudden drops in the load-displacement curves (Figure 14) were due to the sequential detachment of the strengthening layer.

As in the previous strengthening approach, the LC-TRM prevented the fourth hinge to form, meaning that failure occurred again due to formation of three hinges and one additional “release” of the LC-TRM strengthening. The three hinges formed at about 30% of span on the symmetric side to the load application and at both vault springers. Thus, failure occurred at the moment of the “release”. The location of hinges and “release” (R) are depicted in Table 2. Hinge b (Table 2) developed at 23% and 26% of SI1 and SI2 span, respectively, while the “release” (R) developed at 43% of span of both models.

The plate anchors applied to fix the LC-TRM seemed to postpone the full detachment of this layer, but failure occurred when the detachment of the strengthening reached hinge b. Furthermore, crushing of the strengthening mortar at section H was observed in the last cycles (see Figure 15e), which evidences the large deformation achieved at this hinge (hinge b in Table 2). This deformation was also evident on the other side of the hinge (section G in Figure 8d), as the crack presented large opening and depth. As a consequence, the LC-TRM progressively

detached from the intrados until achieving hinge b (Table 2). After this point the strengthening was unable to transfer stresses, leading to failure of the vaults. Rupture of the mesh was observed after the failure of the vaults, as shown in Figure 15f.

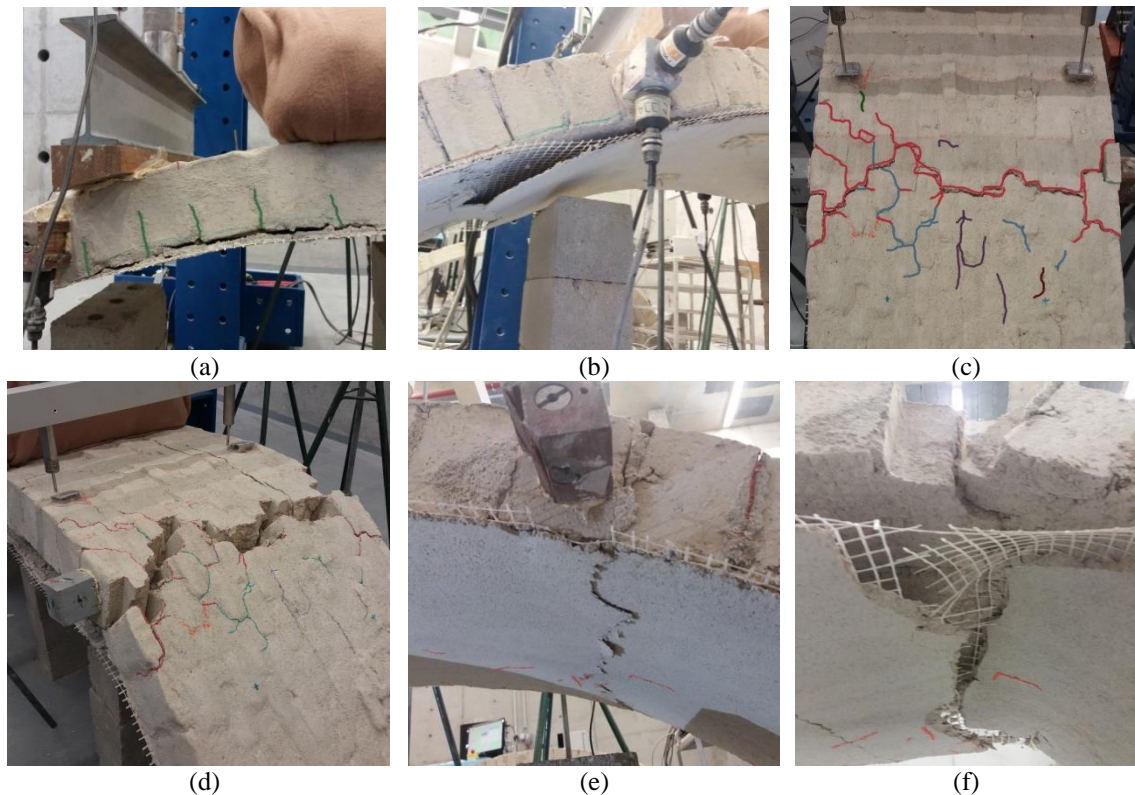


Figure 15. Damage development of the vault models strengthened at the intrados: (a) cracks at section F (SI1); (b) detachment of the strengthening mortar at section F (SI2), (c) cracks at section G before collapse (SI1); (d) cracks at section G after collapse (SI1); (e) mortar crushing at section H (SI2); (f) rupture of fiber-glass mesh at section H (after collapse) (SI2).

4.5 *Repaired vaults strengthened at intrados*

The tests of the repaired vaults included ten loading-unloading cycles. As it can be seen from the cyclic load-displacement curves presented in Figure 16, the structural behavior of both vault models was similar. Regarding the maximum load, DSI1 achieved a value of 1.60 kN in the 6th cycle, while DSI2 achieved a value of 1.35 kN in the 5th cycle. The maximum displacement was of about 22.2 mm and 24.0 mm for DSI1 and DSI2, respectively. The first cracks appeared in the 5th cycle for both tests.

Comparatively to the unstrengthened vault models, the repaired ones attained a small increment of the maximum load. The load capacity increased about 38% and 16% for DSI1 and DSI2, respectively, while the corresponding displacement increased about 2.2 and 1.4 times, respectively. On the other hand, the increase of the maximum displacement was considerable, meaning that the ductility of the vaults seems to increase greatly. In terms of stiffness, no increment was observed (see Section 5.1). Comparatively to the other vault models strengthened at the intrados, the maximum displacement values achieved were very similar, nevertheless the maximum load values of the

repaired vaults were far below. Probably this lack of efficiency of the LC-TRM composite at the intrados was due to the presence of unrepaired damage in the second phase of tests.

The damage development of the repaired vault models is depicted in Figure 17. In general, their failure mechanisms were similar to those of the undamaged vault models strengthened at the intrados. However, small differences in failure mode and crack development were observed. For instance, among the four vault models strengthened at the intrados, only DSI2 presented cracking in section C (Figure 17d), which possibly explains its lower loading capacity. Furthermore, the presence of damage in this section also supports the hypothesis that the damage originated in the first testing phase was not completely repaired.

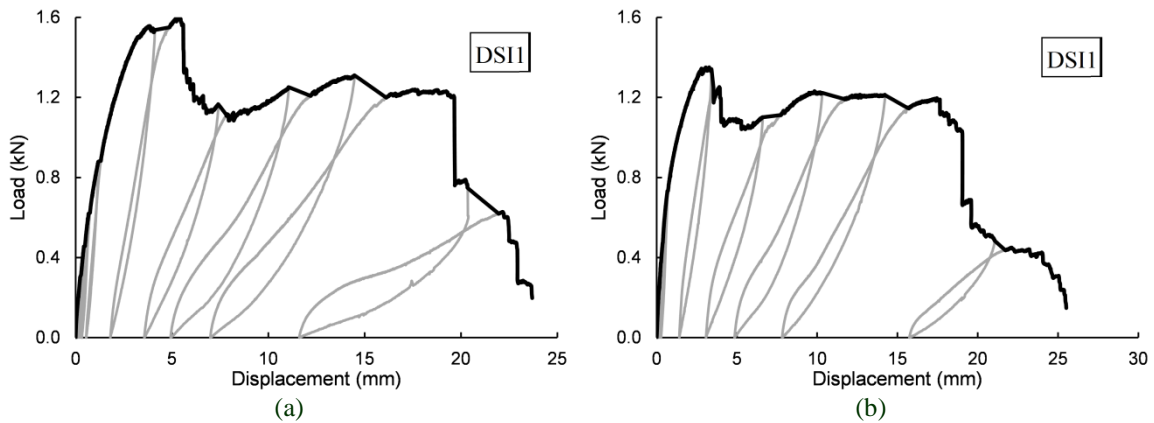


Figure 16. Cyclic load-displacement curves at the loading section and respective envelopes: (a) DSI1; (b) DSI2.

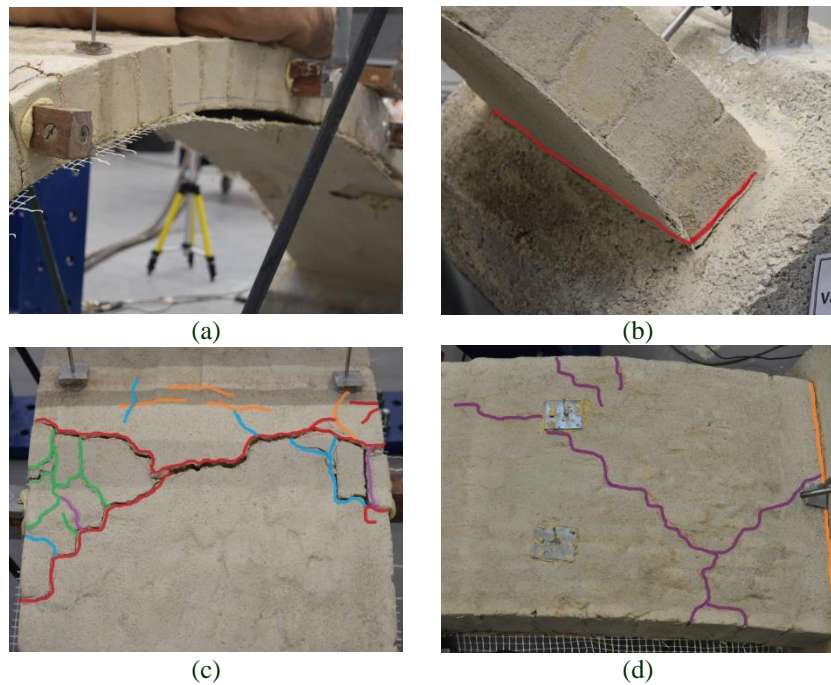
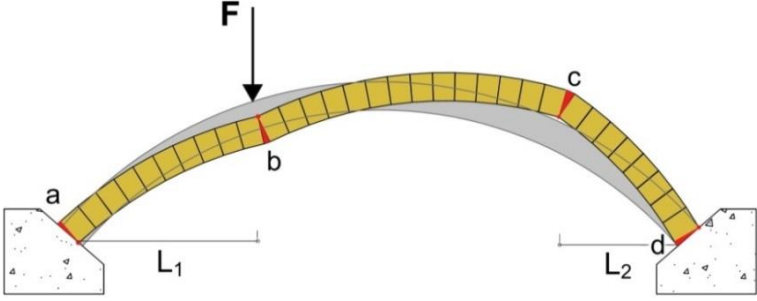
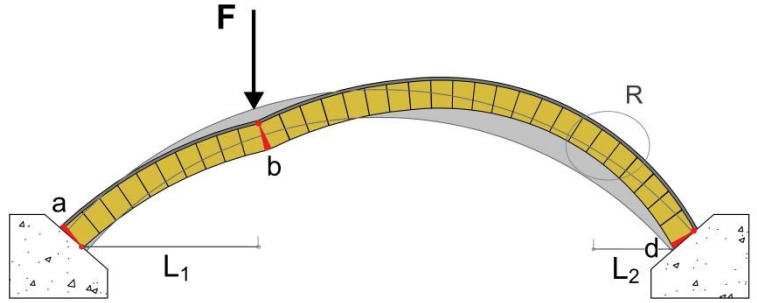
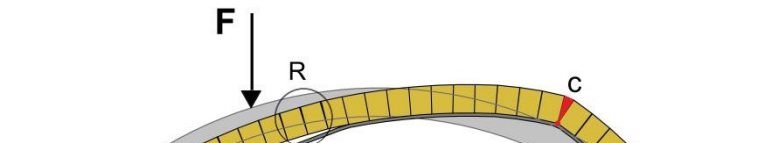



Figure 17. Damage development of the repaired vault models strengthened at the intrados: (a) detachment of the strengthening and progression towards section H (DSI1); (b) cracks at section J (DSI2); (c) cracks at section G (DSI1); (d) cracks at section C (DSI2).

The LC-TRM strengthening applied on the repaired vaults prevented the fourth hinge to fully develop, meaning that the collapse occurred also due to the formation of three hinges and occurrence of an additional “release”. The three hinges developed at the side symmetric to the load application and at both springers. The location of the hinges and “release” (R) are depicted in Table 2. Hinge c (Table 2) developed at 26% and 23% of the span of DSII and DSII2, respectively, while the “release” developed at about 43% of the span of both vaults.

Table 2. Failure mechanisms of the vault models.

<p>Unstrengthened (UN1; UN2)</p>		<p>UN1: $L_1 = 0.32L$ and $L_2 = 0.26L$ UN2: $L_1 = 0.32L$ and $L_2 = 0.23L$</p>
<p>Strengthened at extrados (SE1; SE2)</p>		<p>SE1: $L_1 = 0.32L$ and $L_2 = 0.20L$ SE2: $L_1 = 0.32L$ and $L_2 = 0.11L$</p>
<p>Strengthened at intrados (SI1; SI2)</p>		<p>SI1: $L_1 = 0.43L$ and $L_2 = 0.23L$ SI2: $L_1 = 0.43L$ and $L_2 = 0.26L$</p>
<p>Repaired and strengthened at intrados (DSI1; DSI2)</p>		<p>DSI1: $L_1 = 0.43L$ and $L_2 = 0.26L$ DSI2: $L_1 = 0.43L$ and $L_2 = 0.23L$</p>

Note: R stands for strengthening “release” and L is the span length.

5. Discussion of results

5.1 Global comparison

To provide a general overview of the results of the vaults tested under different strengthening conditions, the eight experimental force-displacement curves are compared in Figure 18. In general, different ductility behaviors were observed. Table 3 presents the relevant points of the aforementioned curves, namely the peak load, 80% of the peak load in the post-peak branch and maximum displacement, as well as the initial stiffness.

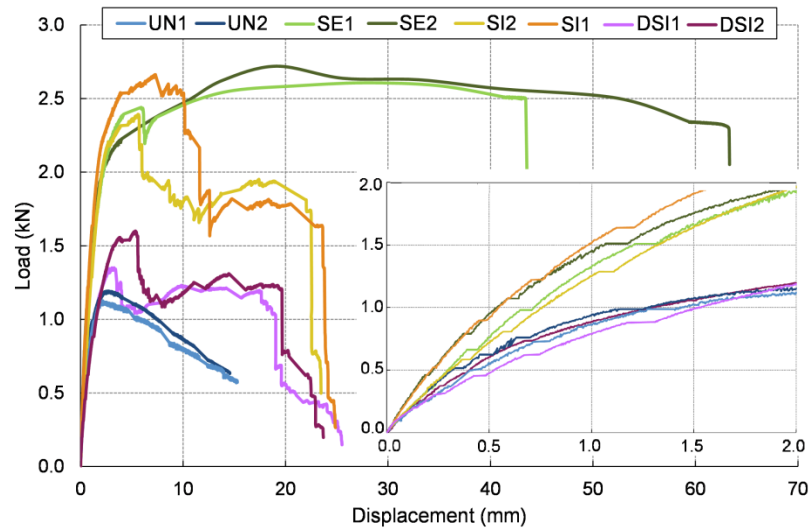


Figure 18. Experimental capacity curves of the vault models (embedded diagram represents the initial part of curves).

Table 3. Relevant points of the experimental curves and initial stiffness of the tested vaults.

Vaults	Peak load		80% of Peak load		Maximum displacement		Initial stiffness [kN/mm]
	Force [kN]	Displacement [mm]	Force [kN]	Displacement [mm]	Force [kN]	Displacement [mm]	
UN1	1.13	2.13	0.84	8.67	0.57	15.30	1.42
UN2	1.19	2.70	0.95	8.27	0.63	14.57	1.57
SE1	2.61	27.67	2.49*	43.44*	2.49	43.44	1.70
SE2	2.72	19.10	2.28*	63.29*	2.28	63.29	2.46
SI1	2.66	7.31	1.84	11.63	1.62	23.63	2.31
SI2	2.39	5.61	1.89	7.96	1.57	22.52	1.67
DSI1	1.60	5.35	1.28	5.79	0.63	22.18	1.30
DSI2	1.35	3.27	1.08	4.02	0.42	23.98	1.57

* The maximum displacement value was assumed, since collapse occurred before 80% of the peak load.

In general, the experimental results show that the LC-TRM composite applied in the vault models improved their structural behavior. This improvement is better quantified in Table 4 in terms of peak load, displacement at 80% of the peak load (post-peak phase), maximum displacement and stiffness, with respect to the average values of the unstrengthened vaults. The vaults strengthened at the extrados achieved the highest increments of load capacity and deformation. Despite that, the undamaged vault models strengthened at the intrados were able to attain load increments similar to those of the ones strengthened at the extrados, though their maximum deformation increments are considerably lower. Regarding the two groups of vaults strengthened at the intrados, it is evident that the damage induced before the repair of DSI1 and DSI2 compromised the peak load increment, while the maximum displacement increment was similar.

Despite the valuable information provided by the maximum displacement values, they may provide a misleading comparison between the failure behaviors of the different groups of vault models. Thus, a further comparison of the displacement at 80% of the peak load in the post-peak branch was performed, when the vaults are expected to be near their collapse limit state. From this comparison, it is possible to observe that the increment introduced by the application of the strengthening at the intrados is low or even negative for the undamaged models and negative for the repaired ones.

Regarding the initial stiffness values of the models, it should be noted that they were computed by means of linear fitting of the loading branch of the first cycle. Generally, it can be stated that strengthening of the undamaged models increased the initial stiffness with respect to the unstrengthened ones. Nevertheless, the scattering and the low number of tested models do not allow to conclude on the strengthening approach providing the highest increment. On the other hand, no significant variation of the initial stiffness was introduced by the repair and strengthening of the unstrengthened vault models with respect to their undamaged condition. Authors consider that more tests have to be performed in order to identify any possible trend relating stiffness variation with the presence of the TRM composite.

Table 4. Relative improvement introduced by the different strengthening approaches

Vaults	Peak load	Displacement at 80% of peak load	Maximum displacement	Initial stiffness
SE1	+125%	+412%*	+191%	+13%
SE2	+134%	+647%*	+324%	+64%
SI1	+129%	+37%	+58%	+54%
SI2	+106%	-6%	+51%	+11%
DSI1	+38%	-32%	+49%	-13%
DSI2	+16%	-53%	+61%	+5%

* The maximum displacement value was assumed, since collapse occurred before 80% of the peak load.

Up to this point, the comparison between the different models took into consideration only the displacement at the loading section, recorded by LVDT2 and LVDT3. Nevertheless, Table 5 presents, in addition, the maxima displacements recorded at the section symmetric to the load application one (LVDT6 and LVDT7), at the springer near support A (LVDT1) and at the springer near support B (LVDT8), for further discussion (see Figure 8a for the location of the LVDTs). At the loading section, all vaults clearly showed a downward displacement. At the section symmetric to the load application one and at the springer near support A, the displacements were upward. In the case of the springer near support B, the displacement was downward for all models. Nevertheless, during the tests of the models strengthened at the extrados and of the repaired models strengthened at the intrados both downward and upward movements were observed, meaning that no clear trend could be established. In general, these observations agree with the expected deformed shape of the different vault models.

In terms of comparison between the maximum displacement values at the different sections of the vault models, it can be observed that the maximum absolute values were recorded at the load application section for the models strengthened at the extrados. In the case of the unstrengthened models and all models strengthened at the intrados, this situation occurred at the section symmetric to

the load application one. The maxima displacements recorded at the springers were in general very low, since they are constrained by the action of the supports and result mainly from the rotation of the hinges formed at these sections. Furthermore, the springer near support B (in Figure 8a) exhibited lower absolute displacements than those of the springer near support A (in Figure 8a), for all models, which can be explained by the higher proximity of the load application section.

Table 5. Maxima displacements recorded at the relevant sections of the vault models (negative values show the upward displacement)

Vaults	Maxima displacements [mm]			
	LVDT2 and LVDT3 (average)	LVDT6 and LVDT7 (average)	LVDT1	LVDT8
UN1	+15.30	-21.84	-1.33	+0.95
UN2	+14.57	-18.60	-1.64	+0.36
SE1	+43.44	-32.94	-2.60	+0.12*
SE2	+63.29	-44.00	-5.94	+0.21*
SI1	+23.63	-29.04	-3.56	+0.76
SI2	+22.52	-30.60	-3.36	+1.26
DSI1	+22.18	-30.53	-1.64	+0.52*
DSI2	+23.98	-30.90	-2.32	+0.11*

* Both downward and upward displacements were observed during the test.

5.2 Bilinear capacity curves of the vault models

In this section, the capacity curves are converted into idealized bilinear backbone curves in order to compare better their behavior in terms of stiffness, strength and ductility. For this purpose, different methods can be found in literature, in which the basic hypothesis is to equalize the energy dissipated under the experimental curve with that under the idealized bilinear diagram up to a predefined ultimate displacement, typically associated to the near collapse limit state. The procedure proposed in REF. [53] is based on the assumption that the displacement corresponding to a 20% loss in capacity is acceptable to be considered as the ultimate limit state. Therefore, the post-peak part of the capacity curve beyond 80% of the peak load shall not be considered for idealizing the bilinear curve. Still according to REF. [53], the displacement corresponding to 70% of the maximum load ($F_{cr} = 0.70F_{max}$) is where the bilinear backbone curve intersects the experimental curve (d_{cr} ; F_{cr}). Therefore, the slope of the idealized bilinear curve (effective stiffness K_e) is calculated as the ratio between F_{cr} and d_{cr} , as given in Eq. (1). Assuming that the elastic stiffness K_y is equal to the effective stiffness K_e allows to compute the strength F_y and the displacement d_y at the limit of the bilinear curve by equalizing the area under the actual and the idealized curve (see Eq. 2).

$$K_e = \frac{F_{cr}}{d_{cr}} = K_y \quad (1)$$

$$\begin{cases} F_y = K_y \times d_y \\ F_y = \frac{E_m}{(d_m - 0.5d_y)} \end{cases} \quad (2)$$

where d_m and E_m are the ultimate displacement and the dissipated energy (area under the actual curve) up to the ultimate displacement, respectively. Figure 19 makes clear the relation between actual and the idealized curve.

The parameters of the bilinear curves idealizing the experimental curves are presented in Table 6. Taking into consideration these curves, the influence of the different strengthening approaches on the strength, stiffness and ductility ($\mu = d_m/d_y$) of the models was further investigated. The models strengthened at the extrados show higher strength capacity increase than those strengthened at the intrados. Furthermore, all strengthening strategies evidenced strength capacity increase with respect to the unstrengthened models.

It should be noted that the collapse of the vault models strengthened at the extrados occurred before reaching 80% of the maximum load. Thus, the displacement corresponding to the 80% of peak load was assumed equal to the maximum displacement. In the models strengthened at the intrados the reduction in strength was rapid due to the sequential detachment of the strengthening. Hence, the displacement corresponding to 80% of the peak load is considerably lower than maximum displacement of the models. This fact corresponds to a reduction in ductility μ (here defined as the ratio between d_m and d_y) of the vault models strengthened at the intrados when compared to the unstrengthened ones.

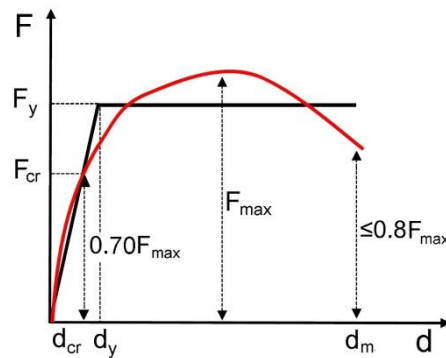


Figure 19. Bilinear idealization of the experimental capacity curve.

Table 6. Parameters of the bilinear curves.

Vaults	F_y [kN]	d_y [mm]	d_m [mm]	k_y [kN/mm]	μ	Stiffness increase	Strength increase	Ductility increase
UN1	1.02	1.12	8.67	0.91	7.7	-	-	-
UN2	1.10	1.05	8.27	1.05	8.9	-	-	-
SE1	2.52	2.43	43.44	1.04	17.9	+6%	+138%	+115%
SE2	2.54	2.43	63.29	1.05	26.1	+7%	+140%	+214%
SI1	2.50	1.93	11.63	1.30	6.0	+33%	+136%	-27%
SI2	2.18	2.00	7.96	1.09	4.0	+11%	+106%	-52%
DSI1	1.56	2.54	5.79	0.61	2.3	-38%	+47%	-73%
DSI2	1.30	1.58	4.02	0.82	2.5	-16%	+23%	-69%

6. Conclusions

This paper presents and discusses the structural performance of a reference vault idealized as representative of the vaulted roofs of the historical adobe houses from Yazd. To this end, an experimental program was conducted by testing eight 1:3 scaled adobe vault models, considering their unstrengthened and strengthened condition. The strengthening adopted consisted of an externally bonded system composed of a low cost fiber-glass mesh covered with an earth-based mortar (LC-TRM). Three strengthening strategies were studied, namely undamaged models strengthened at the extrados, undamaged models strengthened at the intrados and repaired models strengthened at the intrados. The tests were performed under displacement control subjecting the vaults to loading-unloading cycles of increasing amplitude of an imposed vertical displacement at about 30% of the span.

Moreover, in order to capture the damage progress in each test considering the changes in the vault's frequency values, several dynamic identification tests were performed such that a test was done before the first loading (undamaged state) and one after each loading cycle (different damage states). The frequency variation, i.e. the ratio between the frequency of the first mode in the i -th dynamic identification test (f_i) and the initial frequency (f_0) was considered to compare the damage progress.

The experimental results show that the LC-TRM composite improves the initial stiffness, load capacity and displacement capacity. Nevertheless, the level of improvement depends on the strengthening strategy adopted. The experimental behavior of the unstrengthened vaults is characterized by the formation of a typical four-hinge mechanism and low ductility, while the LC-TRM strengthening shown to prevent the full development of the fourth hinge required to form the collapse mechanism. In other words, the strengthened vaults developed only three hinges and one additional "release" associated to the LC-TRM composite.

The results of the dynamic tests show that using the LC-TRM composite at the extrados reduces significantly the slope of the frequency variation (f_i/f_0), implying a best mechanical performance for the SE vaults. For the unstrengthened vaults, the cracks closed after unloading

due to the self-weight, not causing variation on the stiffness and leading to a limited range for the frequency variation.

The application of the strengthening at the extrados provides slightly higher load capacity increment than the application at the intrados. Nevertheless, the deformation capacity increment of the former is much higher. In the case of repaired vaults strengthened at the intrados, the load capacity increment is not so significant, probably due to the extreme difficulty to fully repair the non-visible damage in scaled adobe masonry. Moreover, the repaired vaults present a lower reduction in the frequency variation during the first dynamic tests with respect to the unstrengthened vaults. On the other hand, this strategy seems to provide similar deformation capacity to that considering intrados strengthening in undamaged vaults. The failure of the strengthened vaults is also shown to be controlled by the loss of bond between the strengthening layer and the substrate, which means that improving this property, would probably allow to further exploit the strengthening efficiency of the studied strategies.

As mentioned above, the extrados strengthening showed a better structural performance. However, when planning the strengthening of the vaulted adobe houses in Yazd, the existence of filling over several of the adobe vaults may render the extrados strengthening very invasive to the original structure. Therefore, the application of strengthening at vaults intrados seems to be more feasible in these cases, except for the houses with decorative finishing at vaults intrados.

Finally, the experimental results presented in this paper provide an important and innovative dataset for the calibration of analytical and advanced numerical models for the simulation of the structural performance of adobe vaults.

Acknowledgements

This work was financed by FEDER funds through the Competitively Factors Operational Programme (COMPETE) and by national funds through the Foundation for Science and Technology (FCT) within the scope of projects POCI-01- 0145-FEDER-016737 (PTDC/ECM-EST/2777/2014) and POCI-01-0145-FEDER-007633.

References

- [1] J. Norton, Woodless Construction: Unstabilised earth brick vault and dome roofing without formwork, *Building Issues* 9(2) (1997).
- [2] G.W. Van Beek, Arches and vaults in the ancient Near East, *Scientific American* 257(1) (1987) 78-85.
- [3] T. Mahdi, Performance of traditional arches and domes in recent Iranian earthquakes, 13th World Conference on Earthquake Engineering, Vancouver, B.C., Canada, 2004.
- [4] M.R. Maheri, F. Naeim, M. Mehrain, Performance of Adobe Residential Buildings in the 2003 Bam, Iran, Earthquake, *Earthquake Spectra* 21(S1) (2005) 337-344.
- [5] G. Minke, *Building with Earth: Design and Technology of a Sustainable Architecture*, Birkhäuser Basel, 2006.
- [6] S. Maïni, The French contribution to the reconstruction of Bam and its citadel : diagnosis of damages to vaulted structures Arg-e Bam and Bam town, Iran, International Center for Earth Construction, School of Architecture of Grenoble, 2004.

- [7] S.M. Zahrai, M. Heidarzadeh, Seismic Performance of Existing Buildings During the 2003 Bam Earthquake, 13th World Conference on Earthquake Engineering, Vancouver, Canada, 2004.
- [8] M. Ashtiany, Preliminary Observations on the Bam, Iran, Earthquake of Dec. 26, 2003, Earthquake Engineering Research Institute (EERI), 2004.
- [9] N. Tarque, H. Crowley, R. Pinho, H. Varum, Displacement-Based Fragility Curves for Seismic Assessment of Adobe Buildings in Cusco, Peru, *Earthquake Spectra* 28(2) (2012) 759-794.
- [10] D. Dowling, Adobe housing in El Salvador: Earthquake performance and seismic improvement, in: W.I. Rose, J.B. Bommer, D.L. López, M.J. Carr, J.J. Major (Eds.), *Natural Hazards in El Salvador*, Geological Society of America, U.S.A., 2004.
- [11] E.L. Tolles, F.A. Webster, A. Crosby, E.E. Kimbro, Survey of Damage to Historic Adobe Buildings after the January 1994 Northridge Earthquake, Getty Conservation Institute, Los Angeles, 1996.
- [12] D. Silveira, H. Varum, A. Costa, T. Martins, H. Pereira, J. Almeida, Mechanical properties of adobe bricks in ancient constructions, *Construction and Building Materials* 28(1) (2012) 36-44.
- [13] D. Silveira, H. Varum, A. Costa, Influence of the testing procedures in the mechanical characterization of adobe bricks, *Construction and Building Materials* 40(0) (2013) 719-728.
- [14] A. Eslami, H.R. Ronagh, S.S. Mahini, R. Morshed, Experimental investigation and nonlinear FE analysis of historical masonry buildings – A case study, *Construction and Building Materials* 35 (2012) 251-260.
- [15] S. Bossio, M. Blondet, S. Rihal, Seismic Behavior and Shaking Direction Influence on Adobe Wall Structures Reinforced with Geogrid, *Earthquake Spectra* 29(1) (2013) 59-84.
- [16] A. Figueiredo, H. Varum, A. Costa, D. Silveira, C. Oliveira, Seismic retrofitting solution of an adobe masonry wall, *Materials and Structures* 46(1-2) (2013) 203-219.
- [17] H. Varum, N. Tarque, D. Silveira, G. Camata, B. Lobo, M. Blondet, A. Figueiredo, M.M. Rafi, C. Oliveira, A. Costa, Structural Behaviour and Retrofitting of Adobe Masonry Buildings, in: A. Costa, J.M. Guedes, H. Varum (Eds.), *Structural Rehabilitation of Old Buildings*, Springer Berlin Heidelberg, Berlin, 2014, pp. 37-75.
- [18] R. Illampas, R.A. Silva, D.C. Charmpis, P.B. Lourenço, I. Ioannou, Validation of the repair effectiveness of clay-based grout injections by lateral load testing of an adobe model building, *Construction and Building Materials* 153, 174-184 (2017).
- [19] R. Illampas, Experimental and computational investigation of the structural response of adobe structures, Department of civil and environmental engineering, University of Cyprus, 2013.
- [20] M. Blondet, J. Vargas-Neumann, J. Velásquez, N. Tarque, Experimental study of synthetic mesh reinforcement of historical adobe buildings, in: P.B. Lourenço, P. Roca, C. Modena, S. Agrawal (Eds.), *Structural Analysis of Historical Constructions*, New Delhi 2006, Macmillan India, 2006.
- [21] N. Tarque, Numerical modelling of the seismic behaviour of adobe buildings, ROSE School, Istituto di Studi Superiori di Pavia, Pavia, Italy: Università degli Studi di Pavia, 2011.
- [22] E.L. Tolles, E.E. Kimbro, F.A. Webster, W.S. Ginell, Seismic Stabilization of Historic Adobe Structures Getty Conservation Institute, Los Angeles, 2000.
- [23] M. Como, Statics of historic masonry constructions, Springer, Berlin, 2013.
- [24] U.o.P. UNIPD, NIKER, Deliverable 5.1- Specification for laboratory specimens and testing strategies on floors and vaults., 2013.

- [25] G. Giardina, Studio sul comportamento sismico di archi in muratura., Università degli Studi di Brescia, Brescia, Italy, 2006.
- [26] N. Taranu, G. Oprisan, M. Budescu, G. Taranu, L. Bejan, Improving structural response of masonry vaults strengthened with polymeric textile composite strips, in: O. Martin, X. Zhang (Eds.), Latest Trends on Engineering Mechanics, Structures, Engineering Geology: 3rd WSEAS International Conference on Engineering Mechanics, Structures, Engineering Geology (EMESEG '10) : International Conference on Geography and Geology 2010 (WORLDGEO '10), WSEAS Press, Athens, Greece 2010, pp. 186-191.
- [27] P. Girardello, Rinforzo di volte in muratura con materiali compositi innovativi, Brescia, Italy: Università' Degli Studi di Brescia, 2013.
- [28] D.V. Oliveira, I. Basilio, P.B. Lourenço, Experimental behavior of FRP strengthened masonry arches, *Journal of Composites for Construction* 14(3) (2010) 312-322.
- [29] M.R. Valluzzi, M. Valdemarca, C. Modena, Behavior of brick masonry vaults strengthened by FRP laminates, *Journal of Composites for Construction* 5(3) (2001) 163-169.
- [30] M. Zlamal, P. Stepanek, Strengthening of masonry vaulted structures, Proceedings: CE SB10 Prague - Central Europe towards Sustainable Building 'From Theory to Practice', Czech Technical University in Prague, Prague, Czech Republic, 2010.
- [31] U.S.G.S. USGS, 2014. <https://earthquake.usgs.gov/>.
- [32] N. H. Sadeghi, D.V. Oliveira, M. Correia, H. Azizi-Bondarabadi, A. Orduña, Seismic performance of historical vaulted adobe constructions: A numerical case study from Yazd, Iran, *International Journal of Architectural Heritage* (2018) 1-19.
- [33] N. H. Sadeghi, D.V. Oliveira, M. Correia, H. Azizi-Bondarabadi, A. Orduña, Numerical study on the seismic performance of adobe vaulted architecture: A case study from Iran, *International RILEM Conference on Materials, Systems and Structures in Civil Engineering, Conference segment on Historical Masonry*, Lyngby, Denmark, 2016.
- [34] E. Benvenuto, *La scienza delle costruzioni e il suo sviluppo storico*, Sansoni, Firenze, Italy, 1981.
- [35] J. Heyman, *The masonry arch*, Chichester, Ellis Horwood Limited, U.K., 1982.
- [36] I.V. Carbone, A. Fiore, G. Pistone, *Le costruzioni in muratura-Interpretazione del comportamento statico e tecniche di intervento*, Hoepli, Milan, Italy, 2001.
- [37] L. Nobile, V. Bartolomeo, *Methods for the Assessment of Historical Masonry Arches, Recent advances in civil engineering and mechanics*, WSEAS Press Florence, Italy, 2014.
- [38] I.J. Oppenheim, The masonry arch as a four-link mechanism under base motion, *Earthquake engineering & structural dynamics* 21(11) (1992) 1005-1017.
- [39] M.J. DeJong, *Seismic assessment strategies for masonry structures*, Cambridge, Massachusetts: Massachusetts Institute of Technology, 2009.
- [40] D.V. Oliveira, H. Varum, N. Vicente, O. Sousa, A. Costa, Experimental characterization of the structural response of adobe arches, *TERRA 2012, XI International Conference on the Study and Conservation of Earthen Heritage: "Conservation of Earthen Architectural Heritage against Natural Disasters and Climatic Change"*, Lima, Peru, 2012.
- [41] D. Torrealva, J. Vargas-Neumann, M. Blondet, Earthquake resistant design criteria and testing of adobe buildings at Pontificia Universidad Catolica del Peru, in: M. Hardy, C. Cancino, G. Ostergram (Eds.), *Proceedings of the Getty Seismic Adobe Project 2006 Colloquium*, Getty Conservation Institute Los Angeles, 2006, pp. 3-10.

- [42] N. Sathiparan, K. Meguro, Strengthening of adobe houses with arch roofs using tie-bars and polypropylene band mesh, *Construction and Building Materials* 82 (2015) 360-375.
- [43] CRAterre, Conservation and disaster risk reduction in Ardakan - Tabayi house experience, CRAterre-ENSAG / Hamyaran / Ardakan Municipality / Ardakan District / with the support of the European Union, 2010.
- [44] A. El-Derby, A. Elyamani, The adobe barrel vaulted structures in ancient Egypt: a study of two case studies for conservation purposes, *Mediterranean Archaeology and Archaeometry* 16(1) (2016) 295-315.
- [45] J. Rouhi, A. Aveta, B.G. Marino, A Comparative Analysis (SWOT) of Technical Intervention Plans Carried Out in Sistani House and Payambar Mosque of Bam Citadel, *Mediterranean Journal of Social Sciences* 8(1) (2017) 431.
- [46] M.M. Hejazi, F. Mehdizadeh Saradj, *Persian architectural heritage: Structure*, WIT Press 2014.
- [47] A. Abbass, P.B. Lourenço, D.V. Oliveira, The use of natural fibers in repairing and strengthening of cultural heritage buildings, *Materials Today: Proceedings* (2020).
- [48] N. H. Sadeghi, Conservation and safety assessment of vaulted Adobe Architecture in Yazd, Iran, PhD work performed under the supervision of Professor Daniel V. Oliveira, University of Minho, 2018.
- [49] CEN, EN 1015-11: Methods of test for mortar for masonry, Part 11: Determination of flexural and compressive strength of hardened mortar. European Commission for Standardisation: Brussels., 1999.
- [50] D.V. Oliveira, R.A. Silva, C. Barroso, P.B. Lourenço, Characterization of a Compatible Low Cost Strengthening Solution Based on the TRM Technique for Rammed Earth, *Key Engineering Materials*, Vol. 747, pp. 150-157. DOI: 10.4028/www.scientific.net/KEM.747.150 (2017).
- [51] D. Ewins, *Modal testing: theory, practice and application*, 2nd Edition ed., Research Studies Press LTD, Baldock, Hertfordshire, England, 2000.
- [52] ARTeMIS, Ambient Response Testing and Modal Identification Software, Denmark, 2018.
- [53] NTC., Italian national building code (in Italian). Italy: Ministero delle Infrastrutture e dei Trasporti: Decreto Ministeriale del 17 gennaio 2018, Supplemento ordinario alla G.U. n. 42 del 20 febbraio 2018- Serie generale, 2018.